Published in final edited form as:
Open Infect Dis J. 2008 January 1; 2: 52–58. doi:10.2174/1874279300802010052.

Morphogenesis of Coronavirus HCoV-NL63 in Cell Culture: A Transmission Electron Microscopic Study

Jan M. Orenstein[1,*], **Bridget Banach**[2], and **Susan C. Baker**[2]

[1] Department of Pathology, George Washington University School of Medicine, 2300 Eye Street NW, Washington, DC, USA

[2] Department of Microbiology and Immunology, Loyola University Chicago Stritch School of Medicine, 2160 South First Ave, Maywood, IL, USA

Abstract

NL63 (HCoV-NL63) is a recently discovered human coronavirus that causes respiratory disease in infants and young children. NL63 productively infects LLCMK2 cells and ciliated epithelial cells of human airway cell cultures. Transmission electron microscopic (TEM) studies of NL63 infected LLCMK2 cells revealed that virions are spherical, spiked, and range from 75 to 115 nm in diameter. Virus replication predominantly occurs on the rough endoplasmic reticulum (RER), both perinuclear and cytoplasmic, and the Golgi. Plasma membrane budding was occasionally observed. As virus production increased, aberrant viral forms appeared with greater frequency. Unusual inclusions were present in infected cells including tubular and laminated structures. Pleomorphic double membrane-bound vesicles (DMV), measuring roughly 140 to 210 nm in diameter, were observed. The virus was released via exocytosis and cell lysis. In summary, we report the key morphologic characteristics of NL63 infection observed by TEM analysis.

Keywords

Aberrant; coronavirus; HCoV-NL63; TEM; cell culture

INTRODUCTION

Coronaviruses have recently received increased attention with the outbreak of severe acute respiratory syndrome (SARS-CoV) [1–7] and the discovery of HCoV-NL63, which causes upper and lower respiratory infection in infants and young children [8–12]. The family *Coronaviridae* consists of viruses with a large (25–32 kb) plus strand RNA genome; spikes; envelope, membrane, and nucleocapsid structural proteins. Characteristically the virions are spherical in shape, vary considerably from 60 to 220 nm in diameter, and have a “corona” of club-shaped spikes roughly 20 nm in length [13–20]. Cellular infection by coronaviruses occurs *via* binding to a specific receptor glycoprotein or glycan, and subsequent fusion of the viral envelope with either the plasma membrane or endosomal membranes to release the viral nucleocapsid into the cytoplasm. It is in the cytoplasm where replication occurs. Genomic RNA initially functions as a messenger RNA, then as a template for genome replication. Coronavirus infection yields cellular vacuolization, degeneration, necrosis and sometimes syncytia formation. Progeny virions bud into the lumen of rough endoplasmic reticulum (RER) and Golgi, usurping portions of the organelles unit membrane, which have excluded host cell

*Address correspondence to this author at the Department of Pathology, Ross 502, George Washington University Medical Center, 2300 Eye Street NW, Washington, DC 20037, USA; Tel: 202-994-2943; Fax: 202-994-2618; jorenstein@mfa.gwu.edu.

proteins. Eventually progeny virions accumulate in smooth-walled vesicles which release the virus into the extracellular space through exoctyosis or cell lysis.

The first description, of what is now referred to as HCoV-NL63, came in 2004 from two independent groups in the Netherlands [8,12]. This was followed by an overlapping US study published in 2005 [9]. NL63 is the fourth human coronaviruses described, following the cold viruses HCoV-229E and HCoV-OC43 in the 1960s and SARS-CoV in 2003. NL63 was found in association with acute respiratory disease in infants and young children. Using a PCR method, Esper *et al.* found an incidence of 8.8% of 895 pediatric specimens positive for NL63 over the course of a year [9]. Clinical symptoms associated with infection included: cough, rhinorrhea, tachypnea, fever, abnormal breath sounds (i.e., rhonchi and rales), hypoxia, chest retraction, and wheezing, i.e. upper and lower respiratory tract disease. Subsequently, a French study revealed an incidence of 9.3% from an analysis of 300 samples over the course of 5 months with symptoms that included bronchiolitis, bronchitis, pneumonia, digestive problems, otitis, pharyngitis, and conjunctivitis [11]. NL63 was also found to be associated with the respiratory illness commonly referred to as “croup” in children [21].

Using transmission electron microscopy (TEM), we provide a morphological analysis of NL63 infection of the LLCMK2 cell line.

MATERIALS AND METHODS

HCoV-NL63 and LLCMK2 cells were obtained from Dr. Lia van der Hoek (University of Amsterdam, The Netherlands). The virus was propagated in LLCMK2 cells as previously described [22].

Cells with virus were processed for TEM as previously described [23]. The medium of LLCMK2 cells was replaced with room temperature; pH 7.2-4 cacodylate buffered 4% glutaraldehyde. After at least an hour of fixation, the cells were scraped free with the tip of a disposable plastic pipette and pelleted in a microfuge at 9,500 × g for 5–10 minutes.

Agarose (2% in buffer) was brought to a boil on a hot plate. It was left on the hot plate, while being stirred, so that the agarose remained in a liquid state. The supernatant was carefully aspirated from the pelleted cells. Five to six drops of agarose was added to the cell pellet, gently vortexed to make a homogenous suspension, and microcentrifuge at 9,500 × g for 5–10 minutes. Tubes were kept at 4°C to allow the agarose to solidify (3–4 hours). Using a splintered end of a wooden applicator stick, the pellet was carefully removed from the tube. Excess agar was removed with a razor blade. After processing the agarose block in a microporous processing capsules (Electron Microscopy Sciences, cat. no. 70188), it was be cut into tissue-size pieces for embedding.

A beaker, stir bar, and stirring plate (room temperature) were used for the following steps: the blocks were washed 6 × 10 minutes in buffer, post-fixed in 0.5% osmium tetroxide for 60 minutes, treated for 2 ×10 minutes in 50% ethanol, block stained with 1% uranyl acetate in 50% ethanol for 1 hour, and dehydrated in graded ethanol (70% 3 × 5 minutes, 95% × 10 minutes, and 100% 2 × 10 minutes). The capsules were first placed in propylene oxide for 2 ×10 minutes, then in 50/50 propylene oxide/Spurr’s embedding medium for 1 hour, and finally in 100% Spurr’s for at least 1 hour. The agarose cell pellet blocks were put in the tip of BEEM capsules and polymerize at 70°C for at least 12 hours.

Semithin sections (1 micron) were cut with glass knife and stained with toluidine blue for light microscopic selection of blocks for thin sectioning. Thin sections were stained with uranyl acetate and lead citrate and TEM was performed on a Zeiss EM10 operating at 60kv.

RESULTS

The morphogenesis of HCoV-NL63 was studied in LLCMK2 cell lines using transmission electron microscopy (TEM). Confluent monolayers of LLCMK2 cells were inoculated with 2 $TCID_{50}$ of NL63 and incubated at 33°C. Cells were harvested at 24 hour intervals (days 1–6), and processed for TEM. At day 1 after infection virus production was not evident by visual inspection. By day 2 there was a low level of infection that increased significantly by day 3 and appeared to plateau by days 4 through 6. Approximately 50% of the cells in the culture were productively infected by day 4. It is important to note that in the same cultures, individual cells ranged from displaying no evidence of infection, and apparently healthy, to necrotic cellular debris laced with virions.

Infection of LLCMK2 cells by NL63 revealed morphologic features characteristic of coronavirus infection, as well as some novel cytoplasmic structures. Small numbers of virions were seen at various stages of budding from the plasma membrane, often from villous processes (Fig. 1A, B). Close examination of mouse hepatitis virus (MHV), another coronavirus, also revealed, apparently for the first time, plasmalemmal budding (Fig. 1C, D). However, it was clear that NL63 predominantly replicated in the perinuclear and cytoplasmic rough endoplasmic reticulum (RER) and Golgi (Fig. **2A–E**). The budding could be from either the nuclear or cytoplasmic surface of the perinuclear RER. All productively infected cells revealed the presence of numerous cytoplasmic virus containing vesicles (Fig, **2B**, **E**). Interestingly, it was observed that sometimes the virus and cellular organelles concentrated around the nucleus, as with SARS-CoV [3[, leaving a “swollen” outer cytoplasmic zone containing only ribosomes, intermediate filaments, and microtubules. Multinucleation was rarely observed.

In addition to virus containing vesicles, granular areas of the cytoplasm, consistent with collections of nucleocapsid, were commonly seen (Fig. 2A, E). Sequential steps of envelope acquisition including a nucleocapsid lined membrane, pinching off, and enveloped virion was apparent (Fig. 2E). Furthermore, accumulation of virions in the Golgi, RER, and clear vesicles became increasingly apparent during the course of infection. Virus replication eventually resulted in cell death, which could be either in the form of necrosis and lysis or apoptosis. Virus-laden vesicles ruptured and released their contents into the cytosol.

The typical spherical NL63 virion ranged in diameter from 75 to 115 nm. Occasionally, 20 nm long club-shaped, spikes were clearly seen on the surface of virions (Fig. 3A). The mature particles had a central spherical core, which was either clear, contained electron dense granules (nucleocapsid), or were totally electron dense (Figs. 2D, 3).

Release of coronavirus particles from viable cells appeared to occur through exocytosis (Fig. 4A). Virions were also commonly seen in large collections within complicated surface folds, adjacent to cytoplasmic vesicles, as if they had been released by exocytosis (Fig. 4B). Endocytosis of NL63 within coated pits was readily seen (Fig. 4C).

Of note, as viral infection progressed, virus production was associated with an increasing proportion of pleomorphic, aberrant viral particles (Fig. 4B, 5A, B). Viral aberrancy was first seen as early as day 2 of culture. Particles could be oval, club or rod/bullet shaped, as well as, triangular or diamond shaped. It was not unusual to see open forms of virus, especially with incomplete rings. Sometimes the cytoplasm contained mostly incomplete viral forms.

An unusual feature of NL63 infected cells was the presence of prominent cytoplasmic inclusions. Some had an electron dense coating and contained longitudinally oriented tubules (Fig. 6A). Others consisted of whorls of protein that resembled “myelinoid figures” with 20 nm wide layers of double electron dense outer tracts, a lighter staining ”coating”, and a central thinner electron dense line (Fig. 6B). Lightly-staining tubular structures, measuring

approximately 20 nm in diameter, were sometimes present freely associated with intravacuolar virus (Fig. 6C).

Large aggregates of “capsid” granules (“nucleocapsid inclusions”), often arranged in short rows, and measuring about 20 nm thick, could be seen in close proximity to virus production (Fig. 6D). These collections of granules were free of cytoplasmic organelles.

There were pleomorphic double-membrane vesicles, as seen with MHV [24] and SARS-CoV [25] infections (Fig. 5A, B). They measured in the range of 140 nm to 210 nm in diameter. These DMVs were previously shown to be the site of viral RNA synthesis for coronaviruses [24,25].

DISCUSSION

HCoV-NL63 embodies the morphologic features described for classic human and non-human *Coronaviridae* in terms of size, shape, spikes, aberrant forms, double membrane vesicles, RER and Golgi replication, nucleocapsid granules, and cytopathicity [3,13–15,17–20,24,25]. Not only does NL63 replicate in LLCMK2 cell cultures, but it can also be propagated in ciliated cells of human airway epithelial (HAE) (Banach, *et al.* submitted for publication) cultures similar to SARS-CoV [4].

Morphogenesis of NL63 in LLCMK2 cells takes place on perinuclear RER, cytoplasmic RER, and Golgi. Typical of the *Coronaviridae*, the mature spherical particles varied considerably in size (75 to 115 nm in diameter). The nucleocaspsid material, in mature virions, was either found apposed to the inner surface of the unit membrane or throughout the inside of the particle. Similar to SARS-CoV, granular cytoplasm collections, consistent with nucleocapsid, were present [3]. Multinucleation was rare in our cultures as compared to murine coronavirus mouse hepatitis virus (MHV) in CIF 799 cell lines [17,18] and SARS-CoV [3].

As virus production increased, so did the degree of degeneration, necrosis, and apoptosis of the infected cells. It appeared that as virus production increased, budding started to occur in a “linear” form as if morphogenesis was occurring in an uncontrolled fashion and even possibly on sites other than the RER and Golgi. Sometimes vacuoles containing virus had an electron dense background, as seen with SARS-CoV [3]. It was difficult to capture images consistent with fusion of vacuoles with the plasma membrane and exocytosis of virus from vacuoles, but they clearly did occur. Rarely, one could see mature viral particles in the process of endocytosis into coated vesicles. The optimal time to visualize budding from the plasma membrane was in the early stages of cell infection. This unique observation is also reported, apparently for the very first time, for mouse hepatitis virus (MHV).

A striking feature of NL63 infection of LLCMK2 cells was the presence of many aberrant virion forms which even appeared early in infection, increased over time, and eventually could dominate infected cells. DMVs were not as prominent a feature, as with MHV [24] and SARS-CoV [3,13]. Unusual cytoplasmic structures were also present including oblong inclusions containing linear tubules and “mylenoid” bodies. Lightly staining tubular structures, approximately 20 nm in width, were present in virus-containing vesicles. These three structures appear to be unique to NL63 infection. “Tubuloreticular structures” were not observed [3].

NL63 infection of LLCMK2 cell cultures was distributed throughout the culture, as compared to infection of HAE cell cultures where infection was limited to the supranuclear cytoplasm of ciliated cells (Banach *et al.*, submitted for publication). In addition, NL63 infection of LLCMK2 cells paralleled that of HAE cells in that the process of replication occurred within the RER and Golgi and appeared to be released by exocytosis at the luminal surface. Virions

accumulated near the base of cilia in HAE cultures. As in HAE cultures, increased virus production was associated with cell death and shedding of infected cells.

We report that the ultrastructural features of NL63 infection of LLCMK2 cells parallels the classic characteristics of the *Coronaviridae* family. Virions are spherical, spiked, and range from 75 to 115 nm in diameter. Interesting observations include the extensive array of aberrant viral forms and unusual cytoplasmic structures. We speculate that production of the aberrant forms of membranes and virus particles in NL63 infected cells contributes to the low titers of infectious virus that have been reported [26].

Acknowledgments

The work was supported by funding from NIH HL0892526 (JMO, SCB). We would like to acknowledge the expert technical assistance of Lesley Graham.

References

1. Ksiazek TG, Erdman D, Goldsmith CS, et al. A novel coronavirus associated with severe acute respiratory syndrome. N Engl J Med 2003;348:1953–66. [PubMed: 12690092]
2. Vicenzi E, Canducci F, Pinna D, et al. *Coronaviridae* and SARS-associated coronavirus strain HSR1. Emerg Infect Dis 2004;10:413–8. [PubMed: 15109406]
3. Goldsmith CS, Tatti KM, Ksiazek TG, et al. Ultrastructural characterization of SARS coronavirus. Emerg Infect Dis 2004;10:320–6. [PubMed: 15030705]
4. Sims AC, Baric RS, Yount B, Burkett SE, Collins PL, Pickles RJ. Severe acute respiratory syndrome coronavirus infection of human ciliated airway epithelia: role of ciliated cells in viral spread in the conducting airways of the lungs. J Virol 2005;79:15511–24. [PubMed: 16306622]
5. Peiris JSM, Lai ST, Poon LLM, et al. Coronavirus as a possible cause of severe acute respiratory syndrome. Lancet 2003;361:1319–25. [PubMed: 12711465]
6. Drosten C, Gunther S, Preiser W, et al. Identification of a novel coronavirus in patients with severe acute respiratory syndrome. N Eng J Med 2003;348:1967–76.
7. Rota PA, Oberste MS, Monroe SS, et al. Characterization of a novel coronarvirus associated with severe acute respiratory syndrome. Science 2003;300:1394–9. [PubMed: 12730500]
8. van der Hoek L, Pyrc K, Jebbink MF, et al. Identification of a new human coronavirus. Nat Med 2004;10:368–73. [PubMed: 15034574]
9. Esper F, Weibel C, Ferguson D, Landry ML, Kahn. Evidence of a novel human coronavirus that is associated with respiratory tract disease in infants and young children. J Infect Dis 2005;191:482–8.
10. Choi EH, Lee HJ, Kim SJ, et al. The association of newly identified respiratory viruses with lower respiratory tract infections in Korean children. Clin Infect Dis 2006;43:585–92. [PubMed: 16886150]
11. Vabret A, Mourez T, Dina J, et al. Human coronavirus NL63, France. Emerg Infect Dis 2005;11:1225–9. [PubMed: 16102311]
12. Foucher RAM, Hartwig NG, Bestebroer TM, et al. A previously undescribed coronavirus associated with respiratory disease in humans. Proc Natl Acad Sci USA 2004;101:6212–6. [PubMed: 15073334]
13. Stertz S, Reichelt M, Spiegel M, et al. The intracellular sites of early replication and budding of SARS-coronavirus. Virology 2007;361:304–15. [PubMed: 17210170]
14. Becker WB, McIntosh K, Dees JH, Chanock RM. Morphogenesis of avian infectious bronchitis virus and a related human virus (Strain 229E). J Virol 1967;1:1019–27. [PubMed: 5630226]
15. Hamre D, Kindig DA, Mann J. Growth and intracellular development of a new respiratory virus. J Virol 1967;1:810–6. [PubMed: 4912236]
16. Almeida JD, Tyrrell DAJ. The morphology of three previously uncharacterized human respiratory viruses that grow in organ culture. J Gen Virol 1967;1:175–8. [PubMed: 4293939]
17. Holmes, KV.; Behnke, JN. Evolution of a coronavirus during persistent infection *in vitro*. In: ter Meulen, V.; Siddell, S.; Wege, H., editors. Biochemistry and Biology of Coronaviruses. Plenum Press; New York: 1981.

18. Holmes KV, Frana MF, Robbins SG, Sturman LS. Coronavirus maturation. Adv Exp Med Biol 1984;173:37–52. [PubMed: 6331126]

19. Oshiro LS, Schieble JH, Lennette EH. Electron microscopic studies of coronavirus. J Gen Virol 1971;12:161–8. [PubMed: 4107843]

20. Dubois-Dalcq ME, Doller EW, Haspel MV, Holmes KV. Cell tropism and expression of mouse hepatitis viruses (MHV) in mouse spinal cord cultures. Virology 1982;119:317–31. [PubMed: 6281976]

21. van der Hoek, L.; Sure, K.; Ihorst, G., et al. Croup is associated with the novel coronavirus NL63; PLoS Med. 2005 Aug. p. 1371[serial online][cited 2005 Aug 28]Available from http://medicine.plosjournals.org/perlserv/?request=get-document&doi=10.1371/journal.pmed.0020240

22. Chen Z, Wang Y, Ratia K, Mesecar AD, Wilkinson KD, Baker SC. Proteolytic processing and deubiquitinating activity of papain-like proteases of human coronavirus NL63. J Virol 2007;81:6007–18. [PubMed: 17392370]

23. Graham L, Orenstein JM. Processing tissue and cells for transmission electron microscopy in diagnostic pathology and research. Nature Protocols 2007;2:2439–50.

24. Gosert R, Kanjanahaluethai A, Egger D, Bienz K, Baker SC. RNA replication of mouse hepatitis virus takes place at double-membrane vesicles. J Virol 2002;76:3697–708. [PubMed: 11907209]

25. Snijder EJ, van der Meer Y, Zevenhoven-Dobbe J, et al. Ultrastructure and origin of membrane vesicles associated with the severe acute respiratory syndrome coronavirus replication complex. J Virol 2006;80:5927–40. [PubMed: 16731931]

26. Rowley AH, Baker SC, Shulman ST, et al. Cytoplasmic inclusion bodies are detected by synthetic antibody in ciliated bronchial epithelium during Kawasaki disease. J Infect Dis 2005;192:1757–66. [PubMed: 16235174]

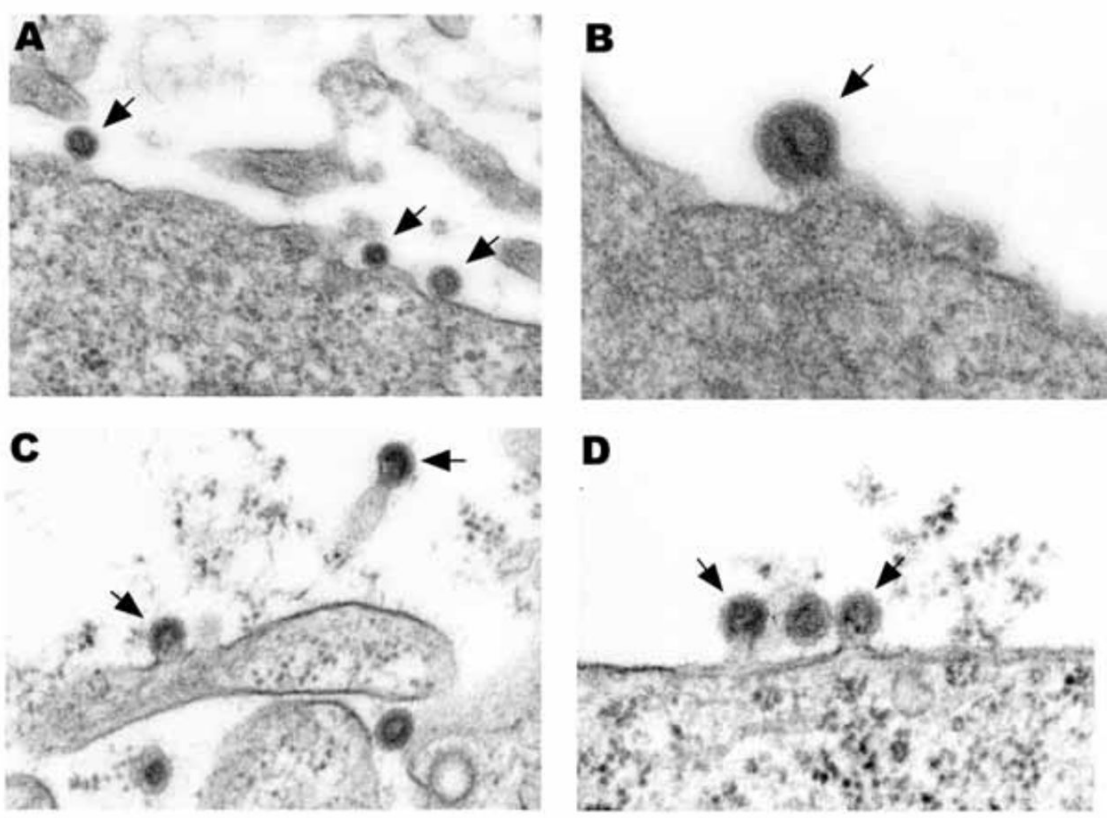

Fig. 1.

(**A**) Three NL63 particles budding from the plasma membrane (arrows). (**B**) A single NL63 particle budding from the plasmalemma (arrow). (**C**) Two MHV particles budding from plasma membrane processes (arrows). (**D**) Two MHV particles budding from the plasmalemma (arrows) flank a particle that has completed budding. **A** × 76,000, **B** × 99,000, **C** × 79,000, **D** × 79,000.

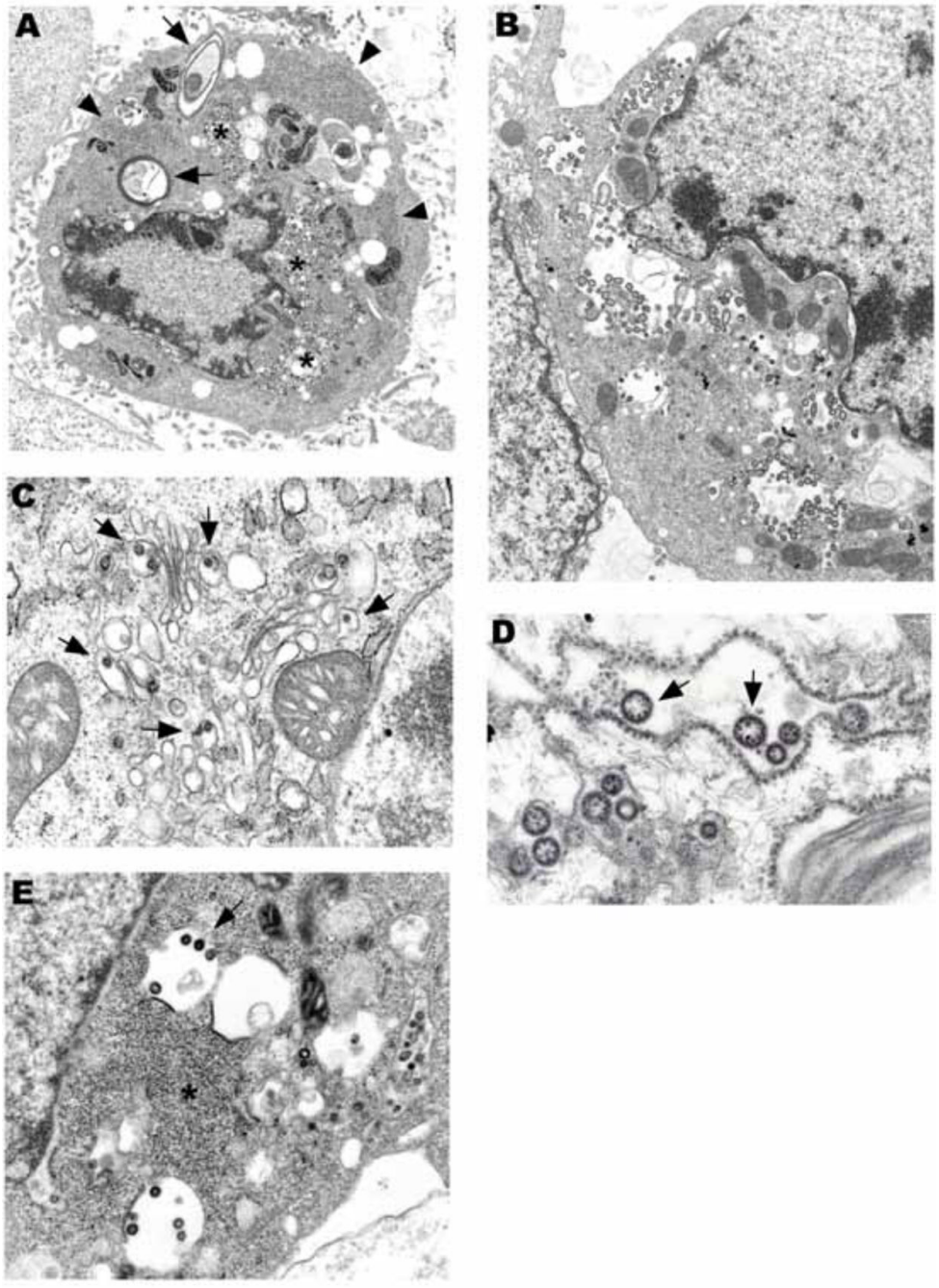

Fig. 2.

(**A**) An electron dense, apoptotic cell rich in virus concentrate around the nucleus (stars). Two laminate bodies are present (arrows). There are several collections of granular nucleocapsid material (e.g., arrowheads). (**B**) Cytoplasmic and perinuclear vacuoles contain abundant virus. (**C**) Virions budding into Golgi cisternae (arrows). (**D**) Ribosomes are in place on a dilated RER cisternae containing virus. Electron dense granular nucleocapsid material can be seen in some of the virions (arrows). (**E**) Virions are budding into smooth membrane vacuoles. **A** × 8,500, **B** × 11,000, **C** × 30,000, **D** × 59,000, **E** × 25,000.

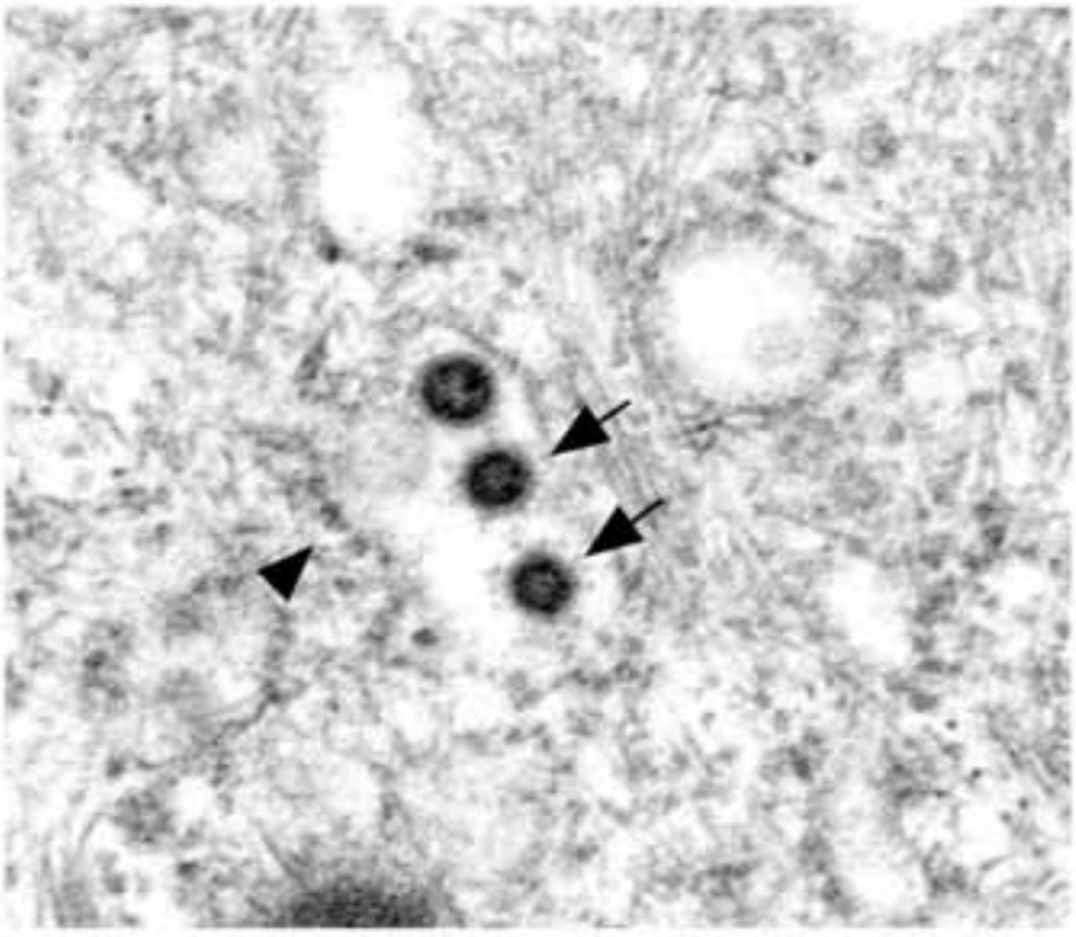

Fig. 3.
Three dense virions are seen in this RER cisternae still partially covered with ribosomes (arrowhead). Two of the virions have detectable spikes (arrows). × 64,000.

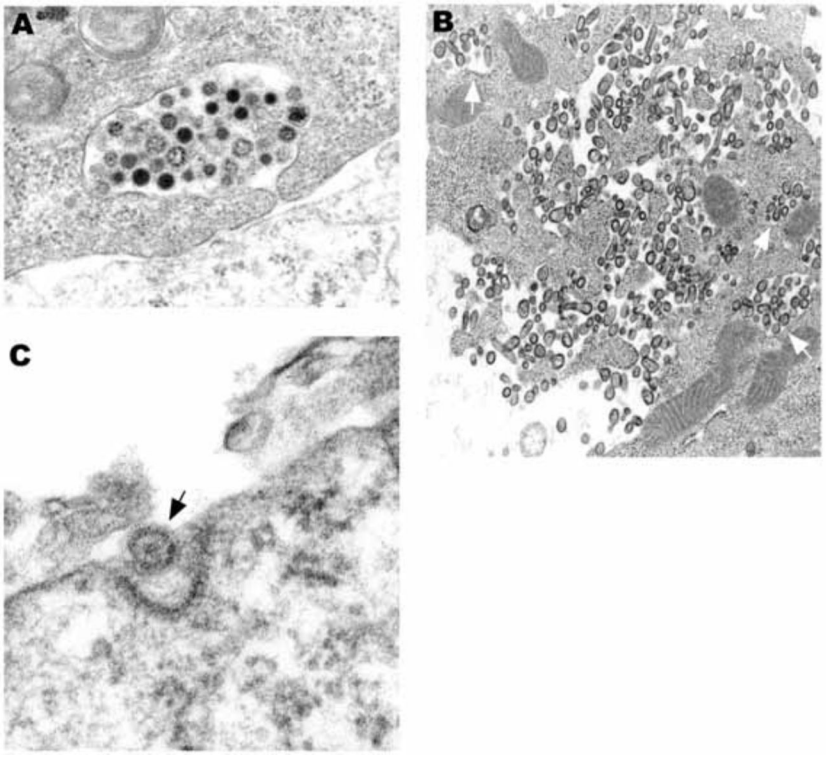

Fig. 4.

(**A**) Virions of varying density appear to be in the process of exocytosis from a healthy cell. (**B**) Virions are in vacuoles (arrows) near the plasma membrane and free trapped within complicated cell processes. The cell appears healthy, suggesting that the free virus was released by exocytosis. Some of the free virions are bullet-shaped. (**C**) A viral particle appears to be in the process of endocytosis in a coated pit. **A** × 50,000, **B** × 29,000, **C** × 120,000.

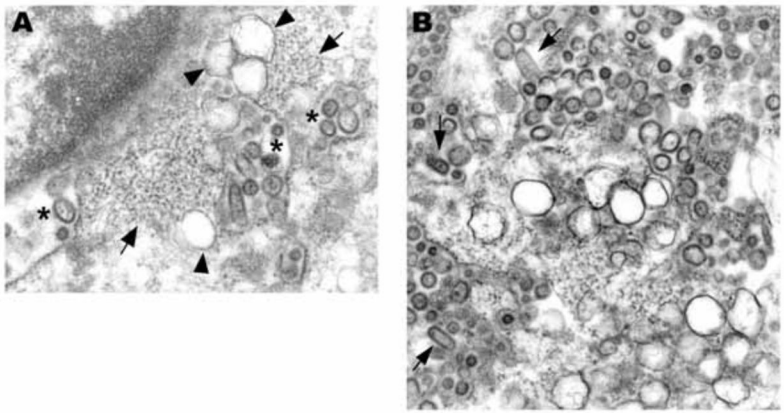

Fig. 5.

(**A**) This perinuclear field shows nucleocapsid material (arrow), vacuoles containing virus (stars), some bullet-shaped, and double-membrane vesicles (arrowheads). (**B**) Numerous double-membrane vesicles are surrounded by abundant viral particles, some bullet-shaped (arrows). **A** × 45,000, **B** × 48,000.

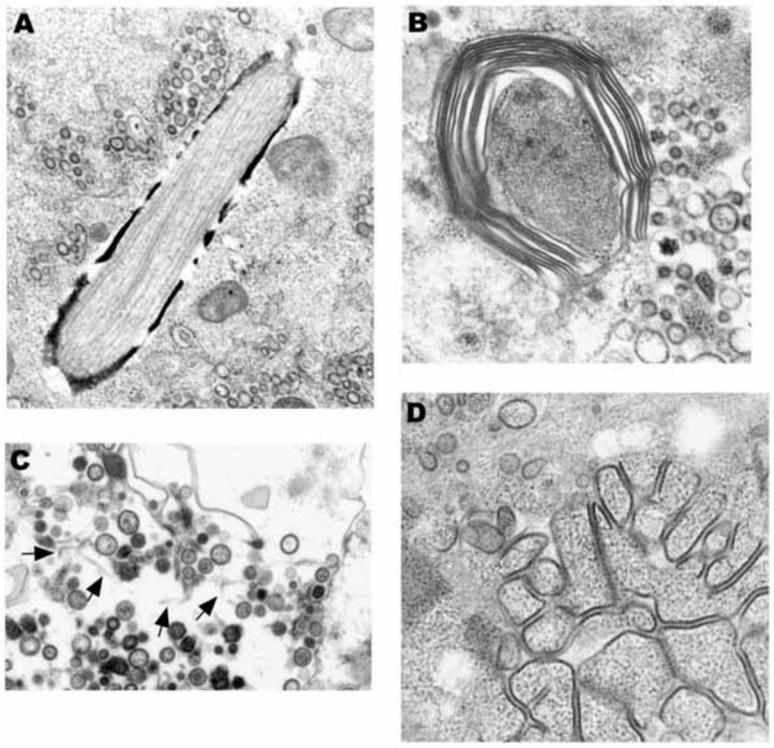

Fig. 6.

(**A**) This unusual inclusions contains longitudinally oriented tubules. Vacuoles containing virus are nearby. (**B**) Periodicity can be seen in a laminated structure that is in close proximity to pleomorphic viral particles (right side). (**C**) In the background are lightly staining tubular structures (arrows). Note the variability in virus diameter. (**D**) Granular nucleocapsid material is associated with electron dense structures that resemble linear arrays of “budding” virus. **A** x36,000, **B** x50,000, **C** x32,000, **D** x44,000.